Applied Physics A (2023) 129:600
https://doi.org/10.1007/s00339-023-06883-9

**Applied Physics A**
**Materials Science & Processing**

# Impact of controlling the barrier height on fabrication of high performance β-$Ga_2O_3$ solar-blind photodetectors

**Thi Kim Oanh Vu[1,2] · Minh Tien Tran[1] · Bui Thi Thu Phuong[1] · Nguyen Thi Minh Hien[1] · Eun Kyu Kim[3]**

Received: 9 June 2023 / Accepted: 27 July 2023 / Published online: 2 August 2023


**Abstract**
Photodetectors based on $Ga_2O_3$ have stimulated extensive attention for diverse applications from civil and military filed. Great progress has been made in the fabrication of $Ga_2O_3$-based photodetector, but they still suffer from their low detectivity. In this study, we present an investigation to achieve ultra-low dark current and high detectivity solar-blind for $Ga_2O_3$-based photodetector by controlling the defect concentration and interface state well with the pulsed laser deposition method. By using pulsed laser deposition, the stoichiometric multi-component film can be obtained. It has been found that the excellent performances of our device (ultrathin thickness of 47 nm) with a low dark current of pA as well as a high sensitivity of $6.25 \times 10^3$ ($I_{photo}/I_{dark}$) are obtained in the as-grown PD under an oxygen pressure of 50 mTorr. Through high temperature annealing of 800 °C and high oxygen pressure of 50 mTorr, the fast response speed (a decay time of 15 ms) is achieved. These are attributed to the co-effect of well-controlled high mobility, reduced oxygen vacancy defects in $Ga_2O_3$ film and increased Schottky barrier height between metal oxide films and metal contact. The electronic transport mechanism in the devices is described in detail to reveal clearly the influence of gas pressure on the optoelectronic properties of photodetectors, which open a promising direction for the development of high-quality economical products.

**Keywords** Barrier height · $Ga_2O_3$ · Solar-blind photodetector · Pulsed laser deposition

## 1 I. Introduction

Optics has seen significant progress for over 100 years. During the twentieth century, with the rapid expansion of photon detection, a need arose for photo detectors that were capable of high-sensitivity, high-responsivity detected the light source. In modern times, photodetectors have become one of the most widespread technologies with numerous practical applications. These range from everyday household devices like video cassette recorder (VCR) remotes and television receivers, to more advanced equipment like charge coupled devices (CCDs) used in video cameras and even radiation detectors capable of detecting sources from the far reaches of the universe. One of the simplest types of sensing applications involves the detection of the presence of an object for security monitoring. Infrared (IR)-detective sensors are widely used for home safety system. With the strong development of communication today, the fiber optic communication systems in which photodetectors generally operate in the IR are most widely used in the market. While in civil and military applications, including flame detection [1],

✉ Thi Kim Oanh Vu
vuthikimoanh92@gmail.com

✉ Eun Kyu Kim
ek-kim@hanyang.ac.kr

Minh Tien Tran
tranminhtien03@gmail.com

Bui Thi Thu Phuong
btphuong@iop.vast.vn

Nguyen Thi Minh Hien
ntmhien@iop.vast.vn

[1] Institute of Physics, Vietnam Academy of Science and Technology, No. 10 Dao Tan, Ba Dinh, Ha Noi, Vietnam

[2] Graduate University of Science and Technology, Vietnam Academy of Science and Technology, Ha Noi, Vietnam

[3] Department of Physics and Research Institute for Natural Sciences, Hanyang University, Seoul 04763, Republic of Korea

missile tracking [2, 3], and intersatellite communications [4], ultraviolet (UV) sensors are more commonly used for electrical arc detection due to their excellent characteristics of intrinsic anti-interference from the visible region [5] and high radiation hardness [6].

The numerous potential applications of photodetectors have led to a considerable amount of interest from researchers, particularly in the development of UV photodetectors (PDs). Researchers have put forth significant effort in fabricating UV and deep ultraviolet (DIVSs) PSs using wide-bandgap semiconductors such as ZnMgO [7], Group (III) metal-nitride compounds like AlGaN/AlN [8], diamond [9], and $Ga_2O_3$ [10] which are well-suited for deep ultraviolet photodetection. Among these materials $Ga_2O_3$ thin films own wide band gap (~ 4.9 eV) with the absorption cutoff wavelength of about 260 nm which covers range of solar-blind region, transparency, high physical and chemical stability, and low cost than diamond and alloy compounds such as AlGaN and MgZnO. These characteristics make $Ga_2O_3$ become a promising candidate for high-performance solar-blind photodetectors. Several methods were used to fabricate $Ga_2O_3$-based photodetectors that has been made by using both physical and chemical methods, typically chemical vapor deposition (CVD) [11, 12], molecular beam epitaxy [13–15], high temperature seed layers [16], and metalorganic vapor-phase epitaxy [17–19]. However, the constructed PDs still had a large dark current, a slow response speed and their decay time was on the order of seconds [20, 21]. The intrinsic defect states and the metal–semiconductor interface are the most important factors influencing PDs quality. Because the high concentration of defects and the low barrier height between metal and semiconductor result in high dark current in photodetectors, which is the primary cause of the observed noise in these devices. Furthermore, the defect states act as traps, capturing generated electron–hole pairs, leading to a sluggish recombination process and a slow speed of the PDs. Otherwise, the concentration of the defects on the surface of semiconductor controls the values of the barrier height between the metal and the semiconductor. We previously demonstrated that oxygen vacancies in $Ga_2O_3$ were one of the main reasons of photodetector photocurrent reduction [26]. Up to date, researchers have focused on improving the responsivity of DUV photodetectors and suppressing oxygen vacancies in $Ga_2O_3$ films [22–24], but the effect of Schottky barrier height on the performance of $Ga_2O_3$ PDs has rarely been reported. Therefore, the investigation of the influence of controlling barrier height and defects on the fabrication of $Ga_2O_3$ plays significant role in achieving high-performance solar-blind PDs. Herein, we use pulsed laser deposition (PLD) technique to fabricate $Ga_2O_3$ thin films, which is considered as an ideal method because it can grow high-quality films at low temperature and well-controlled gas pressure to control the barrier height and reduce defects, and then improve the quality of thin films and response speed of devices.

In this study, we optimize a high-performance β-$Ga_2O_3$ solar-blind photodetector by carefully regulating the concentration of oxygen vacancies and the metal/β-$Ga_2O_3$ barrier height using pulsed laser deposition method and annealing treatment. The photoresponsivity, detectivity, and response time strongly depend on the oxygen gas pressure and annealing temperature. As a result, the β-$Ga_2O_3$-based DUV photodetector fabricated under an oxygen pressure of 30 mTorr and annealing temperature of 800 °C exhibits an excellent detectivity of $10^{13}$ cmHz$^{1/2}$/W and a photoresponsivity of 2.207 A/W. In addition, the response speed of each device is very high and the decay time of PD even decreases to the order of milliseconds, indicating a promising solution for fast-speed PDs in practical applications.

## 2 Experimental method

To grow β-$Ga_2O_3$ thin film on low-cost glass substrate, PLD was used with a 99.99% pure $Ga_2O_3$ target measuring 1 inch in diameter. The deposition process and laser conditions have been described in detail in our previous report [25]. The films were grown at a substrate temperature of 250 °C under varying oxygen pressure for 10 min ranging from 0 to 50 mTorr. Following deposition, the as-deposited β-$Ga_2O_3$ films were annealed in a ceramic tube furnace for 70 min under nitrogen pressure of 10 mTorr at selected temperatures of 500, 600, 700, and 800 °C. Following the annealing process, the films were cooled to room temperature (RT) in preparation for their use in photodetector construction. The photodetectors were then created using a metal–semiconductor-metal structure, which was produced through an evaporation technique. Specifically, two 80-nm-thick Au top electrodes with a channel length of 100 nm were deposited onto the $Ga_2O_3$ during the fabrication process. The whole fabrication process is shown in Fig. 1.

X-ray diffraction (XRD) was employed to examine the crystallinity and orientation of both pre- and post-annealing β-$Ga_2O_3$ thin films in a 2-theta mode. Furthermore, field emission scanning electron microscopy (FESEM) was used to determine the thickness and morphology of the films. The film thickness was measured to be approximately 65 nm, as illustrated in Figure S1 (a). The chemical composition of the $Ga_2O_3$ films was analyzed via X-ray photoelectron spectroscopy (XPS) using monochromatic Kα radiation. Additionally, the steady-state photoluminescence (PL) spectra of the annealed films were recorded with a CCD detector (Andor DV420A-BU2) and a He-Cd laser ($\lambda = 266$ nm) for excitation. A *I–V* test was conducted using a lamp that emitted UV light with a central wavelength of 254 nm, and the *I–V* curves were observed through an HP 4155 analyzer. Finally,

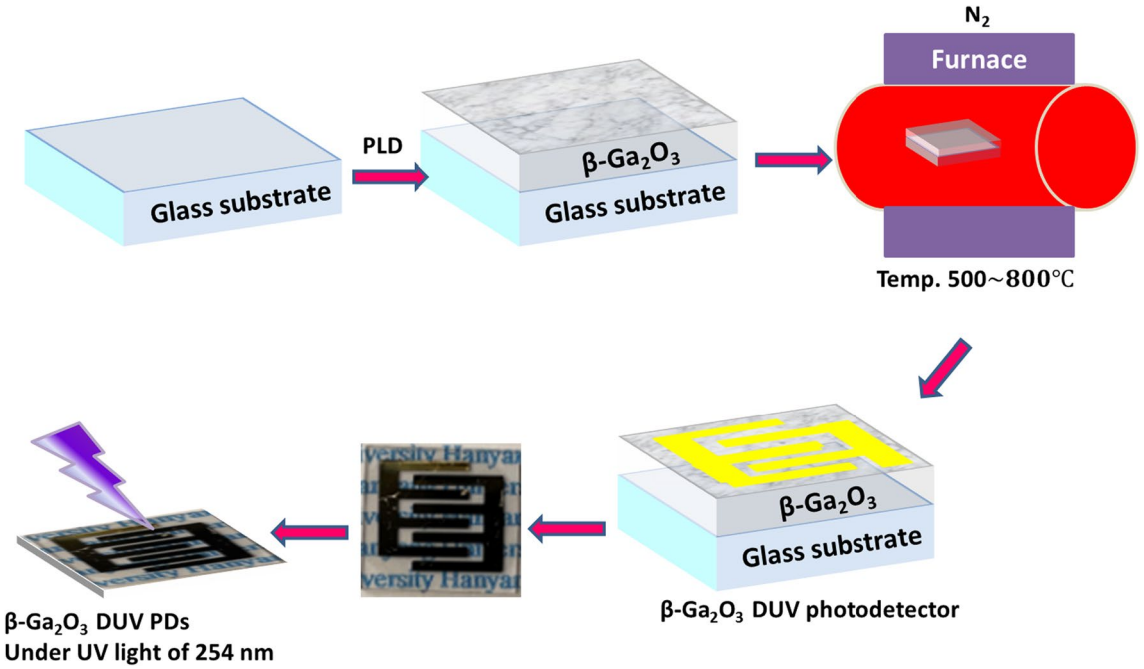


**Fig. 1** The fabrication process of β-$Ga_2O_3$ photodetector with metal–semiconductor-metal (MSM) structure

a monochromator with a wavelength step of a 2 nm was used to determine responsivity ($R$) across DUV to visible wavelength (200–600 nm).

## 3 Results and discussion

### 3.1 Effect of oxygen gas pressure on $Ga_2O_3$ PDs performance

In Fig. 2a, the X-ray diffraction (XRD) curves of β-$Ga_2O_3$ films grown on a glass substrate, under an oxygen pressure of 0–50 mTorr at annealing temperature of 800 °C, are presented. The XRD patterns revealed a broad peak from the glass substrate, in addition to two other peaks at approximately 30.05° and 44.37°. These peaks correspond to the β-$Ga_2O_3$ ($\bar{4}01$) and β-$Ga_2O_3$ (312) planes, respectively (according to JCPDS 76-0573). In our previous report, we studied the influence of oxygen pressure on the structural properties of β-$Ga_2O_3$ films without annealing treatment [25, 26]. The study conducted suggests that the β-$Ga_2O_3$ films, which were prepared at 250 °C without annealing, were either amorphous or microcrystalline. However, during the annealing process, the amorphous films underwent a transformation into a polycrystalline structure. When the partial pressure of oxygen ($P_{O2}$ was increased from 0 to 20 mTorr, there was a significant increase in peak intensity. Conversely, as $P_{O2}$ increased from 20 to 50 mTorr, the intensity gradually decreased. It is believed that an increase in $P_{O2}$ reduces the mobility of adsorbed atoms to their preferred position, resulting in a decline of peak intensity for annealed $Ga_2O_3$ thin films. Figure S1(b) presents the full width at half maximum (FWHM) of the favorable orientation ($\bar{4}01$) and grain size extracted from the FWHM of annealed samples deposited under different oxygen pressures. As the partial pressure of oxygen ($P_{O2}$) increased from 0 to 50 mTorr, there was a decrease in FWHM from 0.057 to 0.034 rad. Additionally, the calculated crystallized size increased from 2.5 to 4.3 nm. This suggests that decreasing deposition pressure is associated with intrinsic defects, such as oxygen vacancies or gallium interstitials in the films, resulting from non-stoichiometric $Ga_2O_3$ film and deteriorating crystallinity. The XRD outcomes indicates that annealing and oxygen are crucial for obtaining high-crystallinity $Ga_2O_3$ thin films. These findings align with our previous research, which demonstrated that $Ga_2O_3$ thin films produced through pulsed laser deposition can be reproduced [22].

The grain size of β-$Ga_2O_3$ was determined using SEM measurements (Fig. 2b–f). The results indicated that at low oxygen pressure, ranging from 0 to 30 mTorr, the grain size was small, and the film surface demonstrated smooth and uniform characteristics. However, when the oxygen pressure increased to 40 and 50 mTorr, the structure began emerge and the grain size of the film expanded. In these two films, several cracks or pinholes were observed, which may be attributed to surface decomposition of the thin film. Another possible explanation is that samples grown under high oxygen pressure encountered collisions between adsorbed-atoms

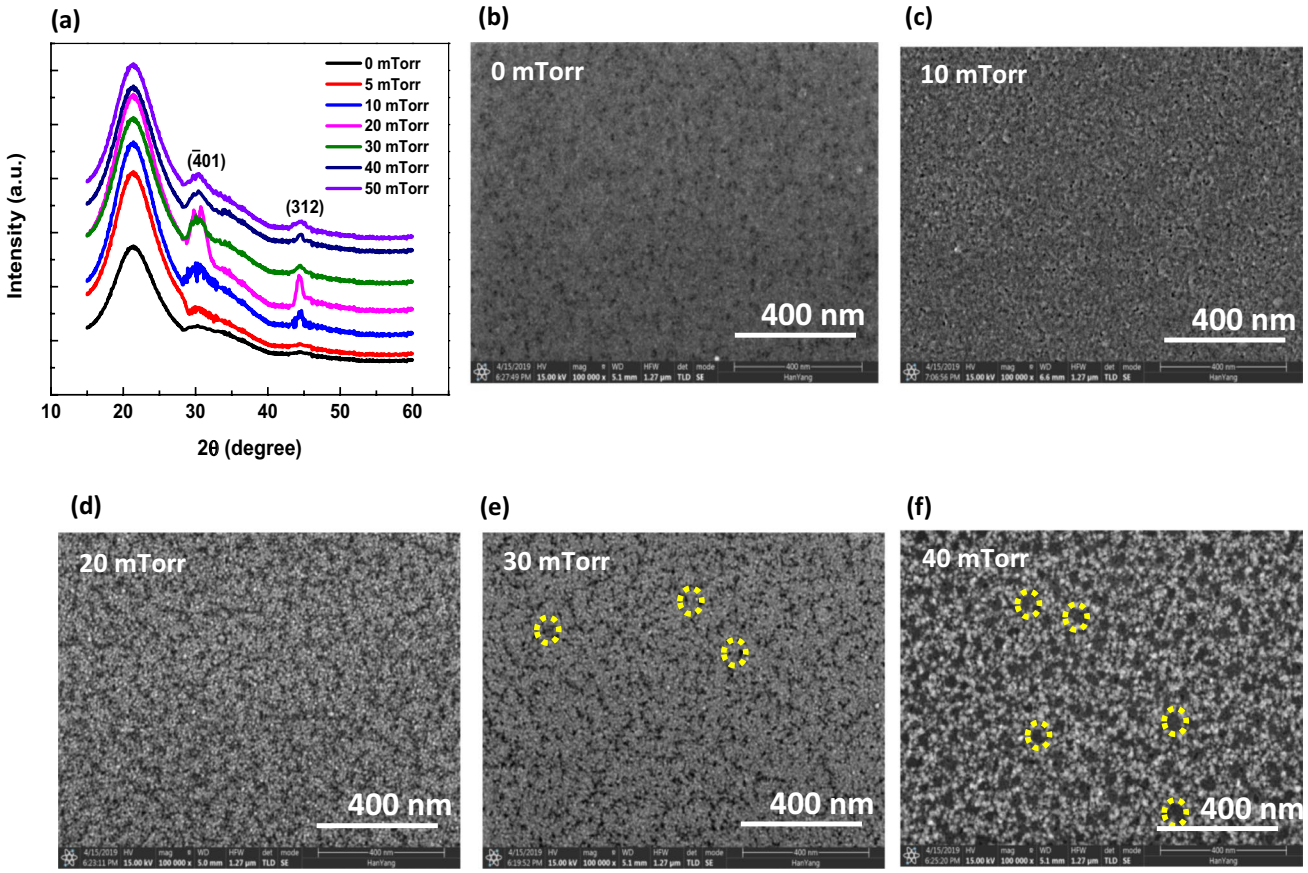


**Fig. 2** **a** X-ray diffraction patterns (Cu Kα radiation) and **b–f** SEM morphology of 800 °C-annealed $GaO_3$ films grown on glass under various oxygen pressures from 0 to 50 mTorr

and gas molecules, thus reducing the requited mobility for a uniform diffusion on substrates, leading to cluster formation [26]. These clusters can agglomerate into masses, resulting in an increase in grain size and the formation of pinholes. The formation of pinholes and cracks may be attributed to a decrease in the photoresponse of the photodetector, which will be further elaborated in the following section.

In Fig. 1, two Au contacts were deposited on the β-$Ga_2O_3$ films to fabricate the PDs devices. Figure 3(a) displays the $I_{dark}$–$V$ characteristics of the post-fabricated β-$Ga_2O_3$ PDs. At an oxygen pressure of 0 mTorr and 25 V, all measured PDs had a low dark current of approximately 10 pA. As the oxygen pressure increased, the dark current of the β-$Ga_2O_3$ film decreased to 1.9 pA at 50 mTorr oxygen pressure. The fabrication of high-sensitivity PD necessitates this low dark current, with the Schottky contact playing a significant role in achieving it. The variation of SBH values with oxygen pressure after annealing is illustrated in Fig. 3b. This figure indicates that the SBH value rises gradually up to approximately 1.02 eV when the oxygen pressure is increased from 0 to 50 mTorr. This value of SBH has a direct impact on the values of dark and photocurrent. Figure 3c depicts the $I_{photo}$–$V$ curves of the PDs when illuminated with 254 light from − 25 to 25 V bias. A noteworthy outcome was observed: at oxygen pressures ranging from 0 to 10 mTorr, the current increased and stayed nearly constant up to 30 mTorr oxygen pressure; it then gradually decreased at oxygen pressure of 40 and 50 mTorr. As a result, we hypothesize that the trend of the $I_{photo}$ curves of the annealed $Ga_2O_3$ films as a function of oxygen can be seen in Figure S1(c). Figure S1(d) indicates the rejection ratio, defined as the $I_{254}/I_{365}$ photocurrent ratio under illumination at 10 V for the samples with and without annealing. The rejection ratio improves significantly from 1.19 to 61 for the annealed PDs when the oxygen flux increases from 0 to 50 mTorr. This increase is more pronounced or the lower the density of oxygen vacancies in the $Ga_2O_3$ films at higher oxygen pressure. Repeated measurements of the photocurrents at different illuminances ($\lambda = 200$–$600$ nm) ensured the reliable responsivity of the PDs. Figure 3d presents the photoresponsivity spectra of PDs under different oxygen pressures at a bias voltage of 25 V. All $Ga_2O_3$ PDs respond selectively to a certain range of DUV wavelength ($\lambda = 225$–$365$ nm), while the photocurrent is negligible at $\lambda > 365$ nm. Notably,

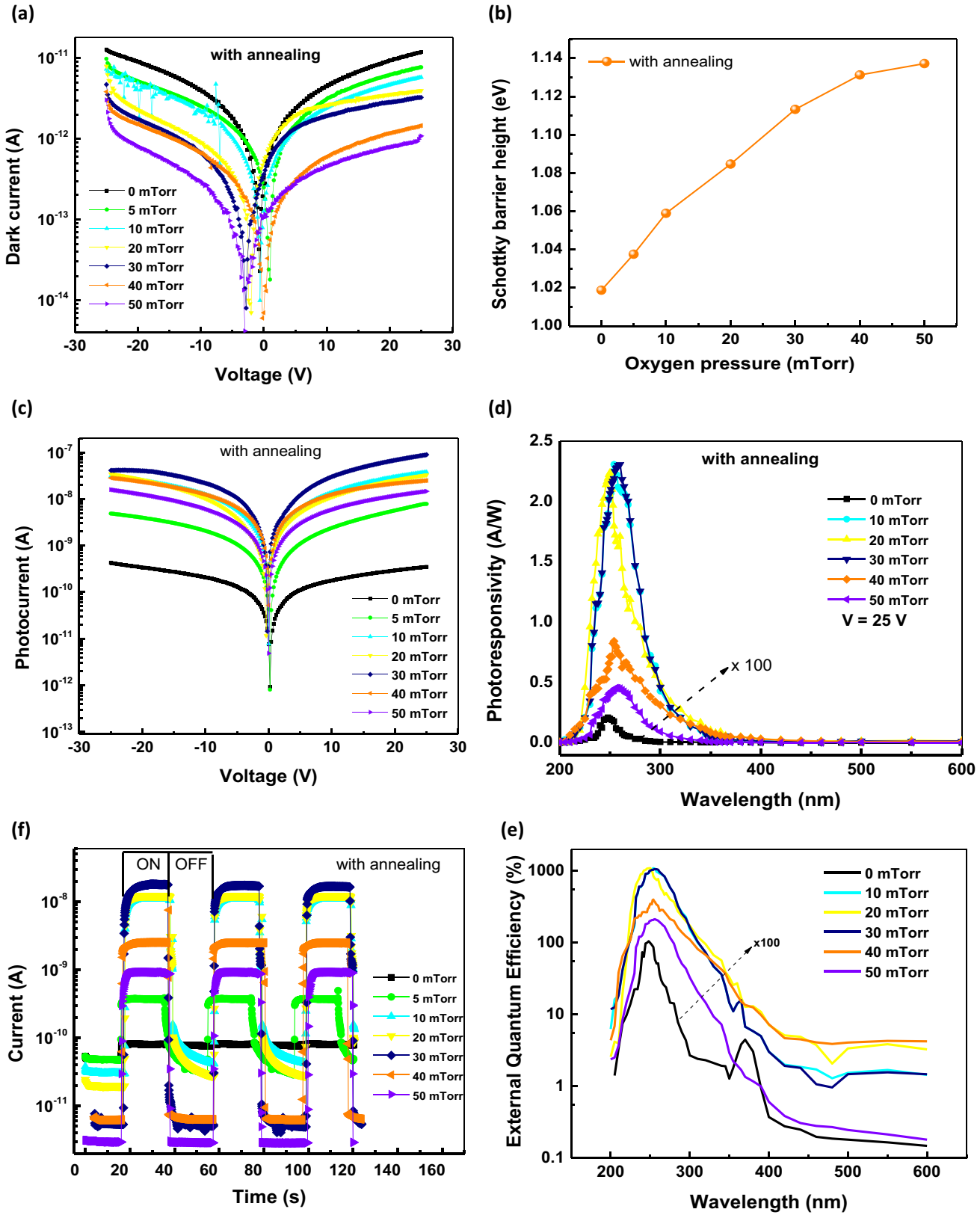


**Fig. 3** **a** Dark *I–V* curves under various oxygen pressures of 800 °C-annealed $GaO_3$ PDs. **b** Schottky barrier height extracted by fitting *I–V* curves as a function of oxygen pressure. **c** Photocurrent–voltage curves under illumination of 254 nm, **d** photoresponsivity spectra, **e** external quantum efficiency as a function of wavelength, and **f** repetitive photo response of 800 °C-annealed $GaO_3$ PDs under various oxygen pressures from 0 to 50 mTorr

although the $Ga_2O_3$ film is ultrathin (about 47 nm in thick), the photoresponsivity obtained here is much higher than that of other previously reported UV detectors [20, 27–29].

As shown in Fig. 3d, the maximal photoresponsivity is affected by oxygen pressure, which is typically similar to photocurrent density. When the oxygen pressure rises from 10 to 30 mTorr, this values remain nearly constant at around 2.207 A/W. Because of the lower density of oxygen vacancy ($V_O$), PDs may be less influenced by entrapment by the photo-generated carriers at greater oxygen fluxes. However, these devices had a higher barrier height, which could prevent photocarrier transport from $Ga_2O_3$ to Au electrodes. As a result, not only the defect concentration in films, but also the SHB, can have an impact on the performance of β-$Ga_2O_3$ PDs. Furthermore, the formation of cracks and pinholes after annealing at high oxygen pressures (40 and 50 mTorr) could result in a decrease in both dark current and photoresponsivity of PDs. Figure 3e depicts the external quantum efficiency (EQE) as a function of incident wavelength retrieved from the responsivity of the PD devices at oxygen pressures ranging from 0 to 50 mTorr. The graph clearly demonstrates that the excellent EQE was obtained at a pressure of 30 mTorr, with a maximum value of 1050%. In addition, there is a noticeable shoulder peak at around 370 nm in β-$Ga_2O_3$ PDs prepared under low oxygen pressure ($P_{O2} < 40$ mTorr). The peak progressively fades when oxygen levels rise due to $V_O$. The predicted photosensitivity of the β-$Ga_2O_3$ PDs with varying oxygen pressure at 25 V is shown in Figure S1 (e). At 30 mTorr, the devices has the highest sensitivity of $9.1 \times 10^3$, which increases with rising oxygen pressure. Figure S1(f) depicts the extracted detectivity $D^*$ of PDs at various oxygen pressures. Although PDs grown at 10, 20, and 30 mTorr achieves an excellent detectivity of about $10^{13}$ cmHz$^{1/2}$/W, which is much better than previous reports on DUV PDs [30–32]. As a results, in addition to attempts to create high responsivity PDs, lowering the dark current of PDs is critical for optimizing device performance. Table 1 summarizes the characteristic parameters of the β-$Ga_2O_3$ PDs under the different oxygen partial pressures. The PD grown at 30 mTorr showed much better optoelectronic performance than the other PDs grown under lower oxygen pressure.

The response of current–time is another key parameter of PDs that is used to measure the response speed and repeatability of $Ga_2O_3$. Until recently, most DUV photodetectors had response times on the order of seconds, limiting their practical application. Figure 3f depicts time-dependent response testing with a 254 nm DUV performed for three cycles at 25 V. Under periodic UV irradiation, all devices displayed good cyclicality. When the UV light is turned on, the current rapidly increases to its maximum value and then stabilizes. When the illumination id turned off, the current drops dramatically. No substantial decrease of PDs was detected, showing that the devices are stable and reproducible. Figure S2 (a)–(g) show the experimental curves of the increase and decrease of the PDs under oxygen pressures ranging from 0 to 50 mTorr. For fitting the photoresponse curve with the bi-exponential relationship equation, the current rise and decay times were taken into account (Supplementary Information). At an oxygen pressure of 0–50 mTorr, the decay times of the devices are 4.5, 1.25, 1.02, 0.81, 0.28, and 0.007 s, respectively. Although the devices fabricated at oxygen pressure of 10, 20, and 30 mTorr and annealed show a significant increase in photocurrent, Photoresponsivity, and detectivity, they still have a long response time that is affected by the persistent photoconductivity (PPC) effect. It should therefore be noted that both the response speed and responsivity must be considered simultaneously for the performance of PD.

### 3.2 Effect of annealing temperature on $Ga_2O_3$ PDs performance

Figure 4a shows the dark current density of the as-grown PDs and the PDs annealed at 500, 600, 700, and 800 °C. We obtained the low dark current PDs both without and with annealing treatment. It is clear that the as-grown device has a higher dark current, indicating a high leakage current. This could be ascribed to the presence of a higher concentration

**Table 1** The characteristic parameters of the β-$Ga_2O_3$ PDs without and with annealing under various temperatures and various oxygen pressures

| | Oxygen pressure (mTorr) | Photocurrent (A/cm$^2$) | Photoresponsivity maximum (A/W) | Sensitivity | Detectivity (cmHz$^{1/2}$/W) | Decay time (s) | |
|---|---|---|---|---|---|---|---|
| | | | | | | $\tau_1$ | $\tau_2$ |
| Without annealing | 50 | $1.71 \times 10^{-3}$ | 5 | $6.25 \times 10^3$ | $1.76 \times 10^{12}$ | 0.033 | 0.10 |
| With annealing | 0 | $1.27 \times 10^{-6}$ | 0.0023 | 2.28 | $4.13 \times 10^7$ | 4.5 | 16 |
| | 5 | $4.05 \times 10^{-5}$ | 0.072 | 101.1 | $2.10 \times 10^{10}$ | 3.25 | 10 |
| | 10 | $3.03 \times 10^{-4}$ | 2.307 | 6600 | $8.88 \times 10^{12}$ | 1.25 | 6.70 |
| | 20 | $3.36 \times 10^{-4}$ | 2.238 | 15,870 | $1.14 \times 10^{13}$ | 1.02 | 6.25 |
| | 30 | $3.57 \times 10^{-4}$ | 2.307 | 27,300 | $1.42 \times 10^{13}$ | 0.81 | 2.00 |
| | 40 | $9.96 \times 10^{-5}$ | 0.84 | 17,100 | $1.38 \times 10^{12}$ | 0.28 | 0.50 |
| | 50 | $5.82 \times 10^{-5}$ | 0.453 | 8130 | $5.50 \times 10^{10}$ | 0.007 | 0.08 |

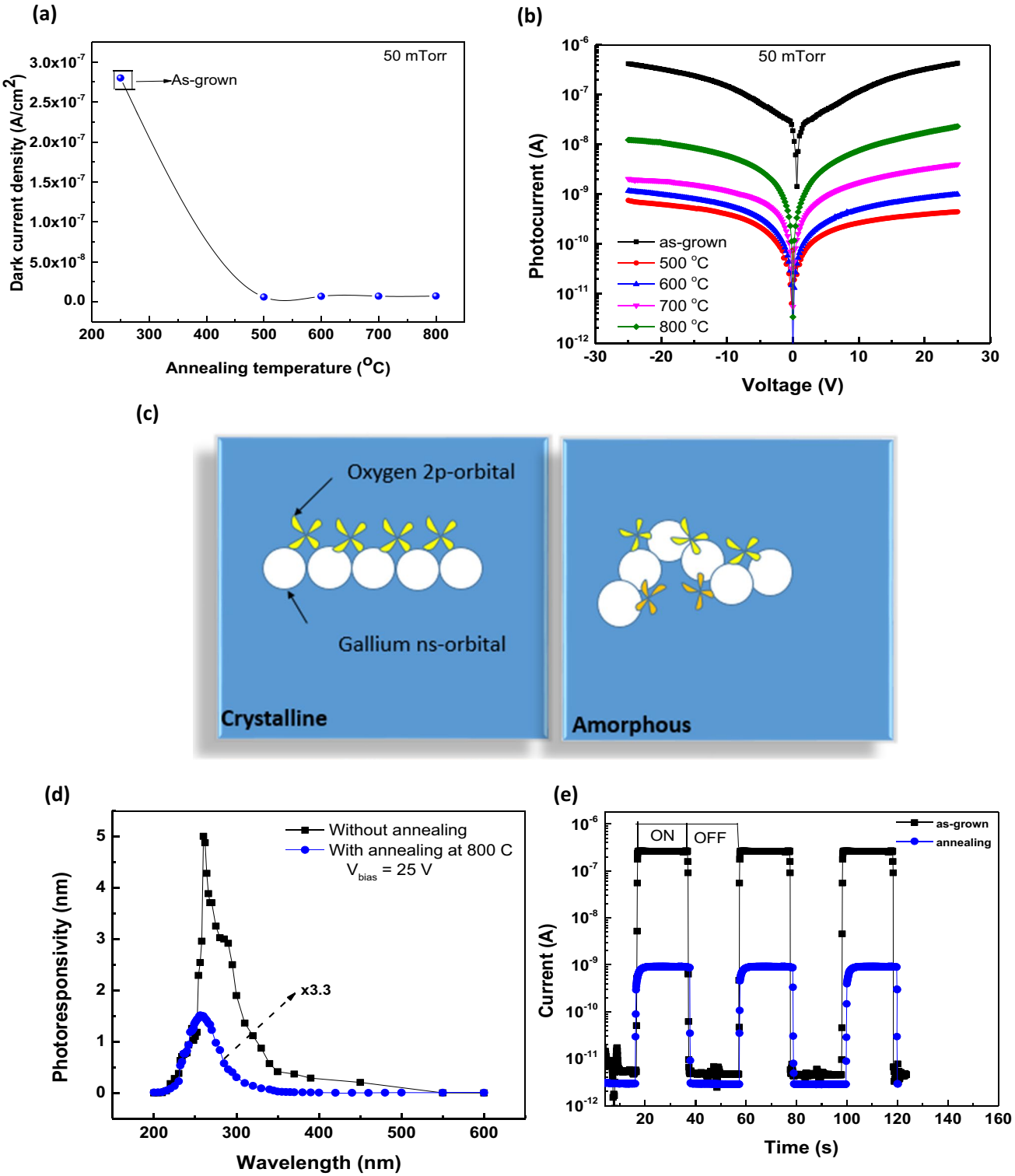


**Fig. 4** **a** Dark current density, **b** photocurrent–voltage curves under illumination of 254 nm as function of annealing temperature of $GaO_3$ PDs under oxygen pressure of 50 mTorr. **c** The influence of disorder on electron orbital overlap in transparent metal oxide. **d** Photoresponsivity spectra and **e** repetitive photo response of as-grown and 800 °C-annealed $GaO_3$ PDs

of intrinsic defects [33] or threading dislocation in the as-grown film than in the annealed one [34]. Another possibility, as mentioned above, is that another different Schottky barrier may play an important role in producing the low dark current of the PDs. The $I_{photo}$–$V$ curves of the PDs under illumination with 254 nm light are is illustrated in Fig. 4b. As the annealing temperature increased, the photocurrent increased. Interestingly, the photocurrent of device fabricated without annealing is approximately 35 times higher than that gained by the device grown with an annealing temperature of 800 °C. It has been reported in research that increasing the annealing temperature could enhance the photocurrent by improving the crystallinity and suppressing defects [35–38]. However, in this study, we fabricated and post-produced samples and investigated that the as-grown PD had a better photoresponse than the PD annealed at a temperature of 800 °C. One of the possibilities is that the mobility in the amorphous transparent conducting oxides (TCOs) materials could be higher than that in commercial crystalline TCOs [39]. The higher electron mobility of these amorphous TCOs is due to the direct overlap of these large and undirected metal atom s-states, as depicted in Fig. 4c [40]. The Schottky barrier height can also be capable of suppressing the photocurrent in PDs. To optimize the performance of PDs, we focus on the comparison between as-grown PD and PD annealed at 800 °C which had a better performance than PDs fabricated at the other annealing temperatures. The rejection ratio defined as the ratio of the photocurrent under illumination with wavelengths of 254 nm and 365 nm ($I_{254}/I_{365}$) at 10 V for the samples without and with annealing at 800 °C, is 48 and 61, respectively. This indicated that the annealing treatment can reduce the defects in the $Ga_2O_3$ thin films and is consistent with previous reports [38, 39]. Repeated measurements of the photocurrents under a range of illumination ($\lambda = 200$–$600$ nm) ensured the reliable responsivity of the PDs.

Figure 4d presents the photoresponsivity spectra of the as-grown and the post-annealed PD devices biased at 25 V. The as-grown sample exhibits the highest photoresponsivity with a maximum of 5 A/W at 260 nm which is much higher than the one obtained after annealing of about 0.45 A/W. The time-dependent photocurrent is shown in Fig. 4e, and all devices are stable after several cycles in the ON/OFF state. The time-dependent photoresponse for one cycle of the untreated and annealed PDs are shown in Figure S3 (a) and (b), respectively. Both the as-grown and annealed $Ga_2O_3$ devices represent a short decay time of 33 and 7 ms, respectively. The fast response of ultra-thin $Ga_2O_3$ PDs in this study makes them competitive in this recent detector market. To optimize the performance of the PDs, we found that the amorphous β-$Ga_2O_3$ film at an oxygen pressure of 50 mTorr is an excellent candidate for fabricating high-speed sensing and high-responsivity PDs. Table 1 summarizes the characteristic parameters of the β-$Ga_2O_3$ PDs deposited on glass substrate without and with annealing. These parameters demonstrated that the amorphous sample exhibited much better optoelectronic performances than the other crystalline PD. This has opened a new interesting research direction: The fabrication of $Ga_2O_3$ thin films at room temperature on a flexible substrate.

### 3.3 Modulation of defects and Schottky barrier height on the performance of PDs

X-ray photoelectron spectroscopy (XPS) was performed for the O 1 s binding energy of the films under varied oxygen pressures and annealed at 800 °C to support the high responsivity and fast photoresponse speed of the amorphous $Ga_2O_3$ PDs (Fig. 5a). Each spectrum in the measured spectra could be deconvoluted into three primary peaks. The lower energy peak (red peak at approximately 530.16 eV) is attributed to oxygen atoms associated with the cations (O–Ga bonds of $Ga_2O_3$), the green peak at approximately 531.17 eV is attributed to $O_x^-$ ($O_2^-$ and $O^-$) ions in oxygen-deficient regions caused by oxygen vacancies, and the higher energy peak (blue peak at approximately 532.1 eV) is attributed to adsorbed oxygen at the surface [41, 42]. It is obvious that the O 1 s peaks vary dramatically as oxygen pressure increases. The intensity of O 1 s at 521 eV decreased as oxygen pressure increased, and the opposite results was found at 532 eV. This means that the higher oxygen pressure reduced the density of $V_O$ while increasing the amount of adsorbed oxygen on the surface. The decrease in $V_O$ with increasing oxygen pressure was also found in films made without annealing [22]. Higher oxygen defect density at lower oxygen pressure was shown to inhibit charge carrier recombination, resulting in a delayed recovery time. Figure 5b shows X-ray photoelectron spectroscopy (XPS) for the O 1 s binding energy of films before and after 800 °C annealing. It is also clear that after annealing, the intensity of O 1 s at approximately 531 eV falls and that at about 532 eV increases, indicating that the concentration of oxygen vacancies ($V_O$) was lowered and the amount of adsorbed oxygen on the surface increased, respectively. When $O_2$ molecules are adsorbed on the surface, they take electrons from conduction bands $E_C$ and trap them on the surface of metal oxides as ions. The formation of an upward band bending and an electron-depleted area increase the barrier height [43]. The presence of more adsorbed oxygen on the surface of films subjected to high oxygen pressure and annealing results in a higher SBH. This effectively limits carrier transport from $Ga_2O_3$ to the Au contact, lowering both the dark current and photocurrent of the corresponding PDs. XPS [42, 44, 45] has proven the effect of oxygen flow on the upward band banding of metal oxides. Therefore, the decrease in photocurrent density of

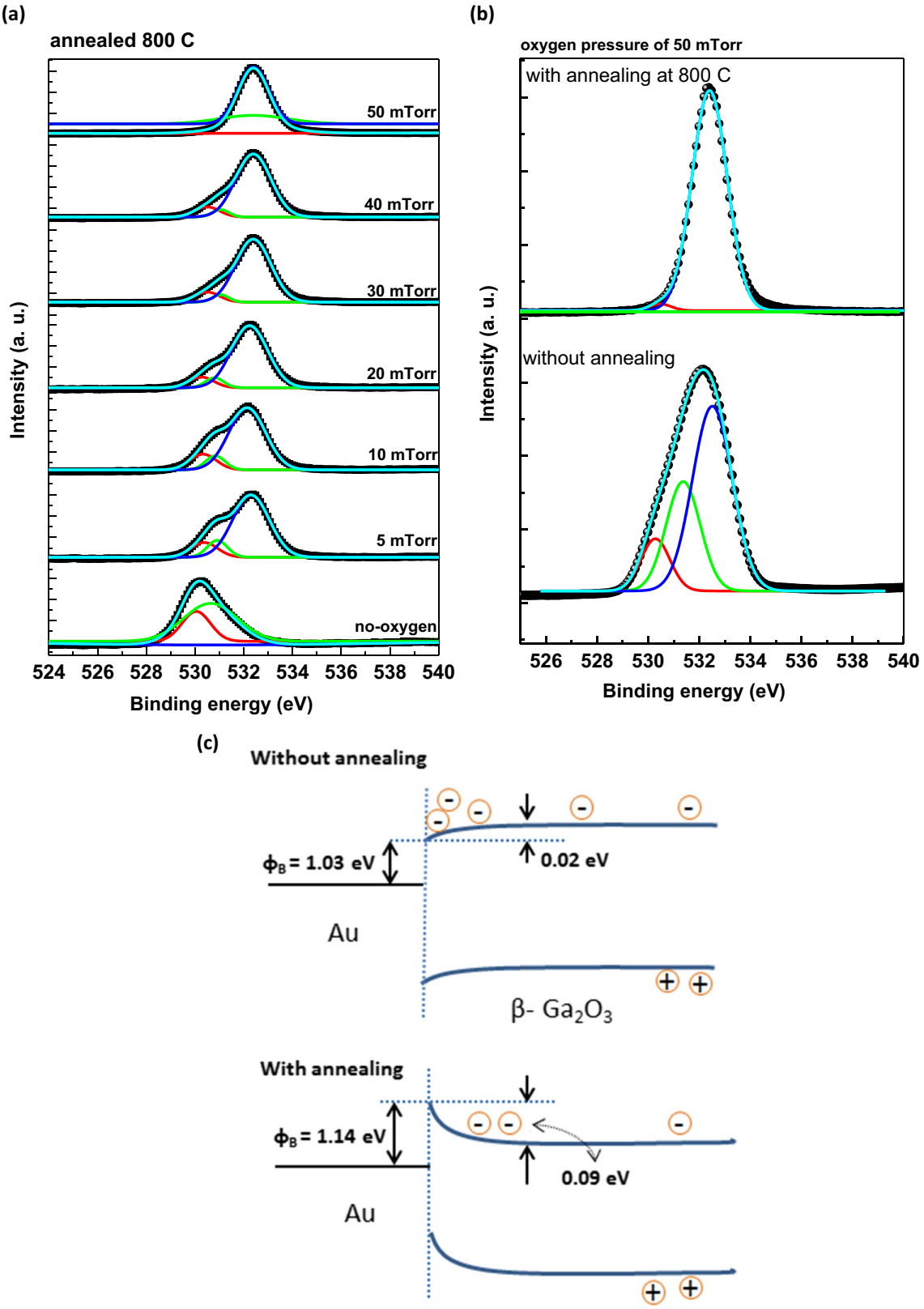


**Fig. 5** Normalized O 1 s XPS spectra for β-$Ga_2O_3$ thin films **a** 800 °C-annealed $GaO_3$ films under various oxygen pressures from 0 to 50 mTorr and **b** without and with annealing at 800 °C. **c** Barrier height of β-$Ga_2O_3$ PDs

annealed PD when oxygen pressure increases from 30 to 50 mTorr might be attributed to SHB augmentation.

To further clarify the discussion above, the carrier transport mechanism and energy band diagram of Au/$Ga_2O_3$ is presented in Fig. 5c. The electron affinity of $Ga_2O_3$ and the work function of Au are about 4.05 eV and 5.1 eV, respectively [43]. The SBH ($\phi_B$) of as-grown sample was approximately 1.047 eV (was also less than 1.05 eV), indicating that the surface energy of the sample bends downward. For the sample annealed at 800 °C and oxygen pressure of 0 and 5 mTorr, the SBH was also less than 1.05 eV, suggesting that the surface energy of these samples also bent decreases. Meanwhile, as the oxygen pressure increases from 10 to 50 mTorr, the SBH is higher than 1.05 eV and the upward curvature increases from 0.01 to 0.09 eV, respectively. Such strong increase blocks the photocurrent transporting from the $Ga_2O_3$ film to the electrodes.

## 4 Conclusion

In conclusion, to fabricate high-performance β-$Ga_2O_3$-based PDs, we have suggested innovative, precisely regulated oxygen pressure and annealing temperatures. The rapid aggregation of clusters caused the grain size of β-$Ga_2O_3$ films to rise with a change in oxygen pressure. The greatest response of 5 A/W, which varied with oxygen pressure and annealing temperature, was attained in as-grown devices at 50 mTorr. At 30 mTorr and 800 °C, post-annealing significantly increased detectivity and response time (decay) to $10^{13}$ cmHz$^{1/2}$/W and 33 ms, respectively. Oxygen vacancy defects in $Ga_2O_3$ films and SHB between $Ga_2O_3$ and metal contacts both contributed to the development of the optoelectrical characteristics of the β-$Ga_2O_3$ PDs. The findings suggest possible methods for producing high-quality solar-blind photodetectors.

**Supplementary Information** The online version contains supplementary material available at https://doi.org/10.1007/s00339-023-06883-9.

**Acknowledgements** This work was supported by the excellent research team development program grant funded by Vietnam Academy of Science and Technology (VAST) (NCXS 02.05/22-23) and in part supported by the National Research Foundation of Korea (NRF) grant funded by the Korea government (MSIT) (NRF-2020R1A4A4078674)

**Author contributions** In this article, the author's contribution are as follow: TKOV: study conception and design, data collection, and manuscript preparation. MTT: data collection and analysis and interpretation of results. BTTP: data collection and analysis and interpretation of results. NTMH: data collection and analysis and interpretation of results. EKK: study conception and design, and manuscript preparation.

**Data availability** Data included in article/supplementary material/referenced in article.

## Declarations

**Conflict of interest** The authors declare no competing financial or non-financial interest to disclose.

## References

1. E.V. Gorokhov, A.N. Magunov, V.S. Feshchenko, A.A. Altukhov, Solar-blind UV flame detector based on natural diamond. Instrum. Exp. Tech. **51**, 280–283 (2008)
2. B. Ouyang, K. Zhang, Y. Yang, Self-powered UV photodetector array based on P3HT/ZnO nanowire array heterojunction. Adv. Mater. Technol. **2**, 1700208 (2017)
3. R. Tang, G. Li, Y. Jiang, N. Gao, J. Li, C. Li, K. Huang, J. Kang, T. Wang, R. Zhang, Predicting the Raman spectra of ferroelectric phases in two-dimensional $Ga_2O_3$ monolayer. ACS Appl. Electron. Mater. **4**, 188–196 (2022)
4. N. Nasiri, R. Bo, F. Wang, L. Fu, A. Tricoli, Ultraporous electron-depleted ZnO nanoparticle networks for highly sensitive portable visible-blind UV photodetector. Adv. Mater. **27**, 4336–4343 (2015)
5. S. Liu, M.-Y. Li, J. Zhang, D. Su, Z. Huang, S. Kunwar, J. Lee, Self-assembled Al nanostructured/ZnO quantum dot heterostructures for high responsivity and fast UV photodetector. Nano-Micro Lett. **12**, 114 (2020)
6. C. Xie, X.T. Lu, X.W. Tong, Z.X. Zhang, F.X. Liang, L. Liang, L.B. Luo, Y.C. Wu, Recent progress in solar-blind deep-ultraviolet photodetector based on inorganic ultrawide bandgap semiconductors. Adv. Funct. Mater. **29**, 1806006 (2019)
7. Z. Guo, D. Jiang, N. Hu, X. Yang, W. Zhang, Y. Duan, S. Gao, Q. Liang, T. Zheng, J. Lv, Significant enhancement of MgZnO metal-semiconductor-metal photodetectors via coupling with Pt nanoparticles surface plasmons. Nanoscale Res. Lett. **13**, 168 (2018)
8. H. So, J. Lim, D. Senesky, Continuous V-grooved AlGaN/GaN surfaces for high-temperature ultraviolet photodetectors. IEEE Sens. J. **16**, 3633–3639 (2016)
9. X. Chang, W.F. Wang, X. Zhang, Z. Liu, J. Fu, S. Fan, R. Bu, J. Zhang, W. Wang, H.X. Wang, J. Wang, UV-photodetector based on NiO/diamond film. Appl. Phys. Lett. **112**, 032103 (2018)
10. S.H. Lee, S.B. Kim, Y.-J. Moon, S.M. Kim, H.J. Jung, M.S. Seo, K.M. Lee, S.-K. Kim, S.W. Lee, High-responsivity deep-ultraviolet-selective photodetectors using ultrathin gallium oxides films. ACS Phot. **4**, 2937 (2017)
11. S. Rafique, L. Han, M.J. Tadjer, J.AJr. Freitas, N.A. Maadik, H. Zhao, Homoepitaxial growth of β-$Ga_2O_3$ thin films by low pressure chemical vapor deposition. Appl. Phys. Lett. **108**, 182105 (2016)
12. S. Kumar, C. Tessarek, G. Sarau, S. Christiansen, R. Singh, Self-catalytic growth of β-$Ga_2O_3$ nanostructures by chemical vapor deposition. Adv. Eng. Mater. **17**, 709–715 (2015)
13. S. Ghose, Md.S. Rahman, Structural and optical properties of β-$Ga_2O_3$ thin films grown by plasma-assisted molecular beam epitaxy. J. Vacuu. Sci. Tech. **34**, 02L109 (2016)
14. D. Guo, Z. Wu, P. Li, Y. An, H. Liu, X. Guo, H. Yan, G. Wang, C. Sun, L. Li, W. Tang, Fabrication of β-$Ga_2O_3$ thin films and solar-blind photodetectors by laser MBE technology. Opt. Mater. Exp. **4**, 1067–1076 (2014)
15. L. Huang, Q. Feng, G. Han, F. Li, X. Li, L. Fang, X. Xing, J. Zhang, Y. Hao, Comparison study of β-$Ga_2O_3$ photodetectors grown on sapphire at different oxygen pressures. IEEE Phot. J. **9**, 6803708 (2017)
16. K. Arora, N. Goel, M. Kumar, M. Kumar, Ultrahigh performance of self-powered β-$Ga_2O_3$ thin film solar-blind photodetector

grown on cost-effective Si substrate using high-temperature seed layer. ACS Phot. **5**, 2391–2401 (2018)
17. Z. Hu, Q. Cheng, T. Zhang, Y. Zhang, X. Tian, Y. Zhang, Q. Feng, W. Xing, J. Ning, C. Zhang, J. Zhang, Y. Hao, Solar-blind photodetectors fabricated on β-$Ga_2O_3$ films deposited on 6° off-angled sapphire substrate. J. Luminesc. **255**, 119596 (2023)
18. R. Xu, X. Ma, Y. Chen, Y. Mei, L. Ying, B. Zhang, H. Long, Mater. Sci. Second. Process. **144**, 106621 (2022)
19. M. Baldini, M. Albrecht, D. Gogova, R. Schewski, G. Wagner, Effect of indium as a surfactant in $(Ga_{1-x}In_x)_2O_3$ epitaxial growth on β-$Ga_2O_3$ by metal organic vapour phase epitaxial. Semicond. Sci. Tech **30**, 024013 (2015)
20. T. Oshima, T. Okuno, S. Fujita, Ga2O3 thin film growth on c-plane sapphire substrates by molecular beam epitaxy for deep-ultraviolet photodetectors. Jpn. J. Appl. Phys. **46**, 7217–7220 (2007)
21. L.X. Qian, Y. Wang, Z.H. Wu, T. Sheng, X.Z. Liu, β-$Ga_2O_3$ solar-blind deep-ultraviolet photodetctor based on annealed sapphire substrate. Vacuum **140**, 106–110 (2017)
22. S. Bhowmick, R. Saha, M. Mishra, A. Sengupta, S. Chattopadhyay, S. Chakrabarti, Oxygen mediated defect evolution in RF sputtered $Ga_2O_3$ thin films on p-Si substrate. Mater. Today Commun. **33**, 104766 (2022)
23. L. Gu, H.-P. Ma, Y. Shen, J. Zhang, W.-J. Chen, R.-Y. Yang, F. Wu, L. Yang, Y.-X. Zeng, X.-R. Wang, J.-T. Zhu, Q.-C. Zhang, Temperature-dependent oxygen annealing effect on the properties of $Ga_2O_3$ thin film deposited by atomic layer deposition. J. Alloy. Comp. **925**, 166727 (2022)
24. T. Fan, N. Tang, J. Weii, S. Zhang, Z. Sun, G. Li, J. Jiang, L. Fu, Y. Zhang, Y. Yuan, X. Rong, W. Ge, X. Wang, Reduction of vacancy defects induced by thermal annealing in β-$Ga_2O_3$ epilayer. Micro Nanostruct. **176**, 207525 (2023)
25. T.K.O. Vu, D.U. Lee, E.K. Kim, The enhancement mechanism of photo-response depending on oxygen pressure for $Ga_2O_3$ photodetectors. Nanotechnology **31**, 245201 (2020)
26. T.K.O. Vu, D.U. Lee, E.K. Kim, The effect of oxygen partial pressure on band gap modulation of $Ga_2O_3$ grown by pulsed laser deposition. J. Alloy. Comp. **806**, 874–880 (2019)
27. A.S. Pratiyush, S. Krishnamoorthy, S.V. Solanke, Z. Xia, R. Muralidharan, S. Rajan, N.D. Nath, High responsivity in molecular beam epitaxy grown β-Ga2O3 metal semiconductor metal solar blind deep-UV photodetector. App. Phys. Lett. **110**, 221107 (2017)
28. F.P. Yu, S.L. Ou, D.S. Wuu, Pulsed laser deposition of gallium oxides films for high performance solar-blind photodetector. Opt. Mater. Express **5**, 1240 (2015)
29. Z. Hajnal, J. Miró, G. Kiss, F. Réti, P. Deák, R.C. Herndon, J.M. Kuperberg, Role of oxygen vacancy defect states in the n-type conduction of β-$Ga_2O_3$. J. Appl. Phys. **86**, 3792–3796 (1999)
30. G. Schmitz, P. Gassmann, R. Franchy, A combined scanning tunneling microscopy and electron energy loss spectroscopy study on the formation of thin, well-ordered β-$Ga_2O_3$ films on CoGa(001). J. Appl. Phys. **83**, 2533–2538 (1998)
31. B. Zhao, F. Wang, H. Chen, Y. Wang, M. Jiang, X. Fang, D. Zhao, Solar-blind avalanche photodetector based on single ZnO-$Ga_2O_3$ core-shell mocrowire. Nano Lett. **156**, 3988–3993 (2015)
32. M. Yu, C. Lv, J. Yu, Y. Shen, L. Yuan, J. Hu, S. Zhang, H. Cheng, Y. Zhang, R. Jia, High-performance photodetector based on sol-gel epitaxial grown a/β-Ga2O3 thin films. Mater. Today Commun. **25**, 101532 (2020)
33. M. Heinemann, J. Berry, G. Teeter, T. Unold, D. Ginley, Oxygen deficiency and Sn doping of amorphous $Ga_2O_3$. Appl. Phys. Lett. **108**(2), 022107 (2016)
34. J. Carrano, T. Li, P. Grudowski, C. Eiting, R. Dupuis, J. Campbell, Comprehensive characterization of metal-semiconductor-metal ultraviolet photodetectors fabricated on single-crystal GaN. J. Appl. Phys. **83**(11), 6148–6160 (1998)
35. P. Gu, X. Zhu, D. Yang, Effect of annealing temperature on the performance of photoconductive ultraviolet detectors based on ZnO thin film. Appl. Phys. A **125**, 50 (2019)
36. F. Yi, Q. Liao, X. Yan, Z. Bai, Z. Wang, X. Chen, Q. Zhang, Y. Huang, Y. Zhang, Simple fabrication of a ZnO nanorod array UV detector with a high performance. Phys. E Low-Dimens. Syst. Nanostruct. **61**, 180–184 (2014)
37. Y.Y. Zhang, L.X. Qian, Z.H. Wu, P.T. Lai, X.Z. Liu, Improved performance of amorphous ingamgo metal-semiconductor-metal ultraviolet photodetector by post deposition annealing in oxygen. IEEE Trans. Nanotechnol. **17**, 29–35 (2018)
38. J. Yu, Z. Nie, L. Dong, L. Yuan, D. Li, Y. Huang, L. Zhang, Y. Zhang, R. Jia, Influence of annealing temperature on structure and photoelectrical performance of β-$Ga_2O_3$/4H-SiC heterojunction photodetector. J. Alloy Comp. **798**, 458–466 (2019)
39. A.J. Leenheer, J.D. Perkins, M. Van Hest, J.J. Berry, R.P. Ohayre, D.S. Ginley, General mobility and carrier concentration relationship in transparent amorphous indium zinc oxide films. Phys. Rev. B **77**, 115215 (2008)
40. H. Hosono, N. Kikuchi, N. Ueda, H. Kawazoe, Working hypothesis to explore novel wide band gap electrical conducting amorphous oxides and examples. J. Non-crystall. Solid **200**, 165–169 (1996)
41. S. Chen, M.E.A. Warwick, R. Binions, Effect of film thickness and thermal treatment on the structural and optoelectronic properties of Ga-doped ZnO films deposited by sol-gel method. Sol. Energy Mater. Sol. Cells **137**, 202–209 (2015)
42. Y. Tu, S. Chen, X. Li, J. Gorbaciova, W.P. Gillin, S. Krause, J. Briscoe, Control of oxygen vacancies in ZnO nanorods by annealing and their influence on ZnO/PEDOT:PSS diode behavior. J. Mater. Chem. C **6**, 1815–1821 (2018)
43. C. Wang, L. Yin, L. Zhang, D. Xiang, R. Gao, Metal oxide gas sensors: sensitivity and influencing factors. Sensors **10**(3), 2088–2016 (2010)
44. O. Bierwagen, J.S. Speck, T. Nagata, T. Chikyow, Y. Yamashita, H. Yoshikawa, K. Kobayashi, Depletion of the $In_2O_3$ (001) and (111) surface electron accumulation by an oxygen plasma surface treatment. Appl. Phys. Lett. **98**, 172101 (2011)
45. M. Mohamed, K. Irmscher, C. Janowitz, Z. Galazka, R. Manzke, R. Fornari, Schottky barrier height of Au on the transparent semiconducting oxide β-$Ga_2O_3$. Appl. Phys. Lett. **101**, 132106 (2012)